Computation of enhanced turbulent heat transfer in a channel with periodic ribs

W.B. Tsai and W.W. Lin
Department of Mathematics, National Tsing-Hua University, Hsinchu, Taiwan and
C.C. Chieng
Department of Engineering and System Science, National Tsing-Hua University, Hsinchu, Taiwan

Received November 1998
Revised June 1999
Accepted September 1999

Keywords *Heat transfer, Fluids, Flow, Turbulence, Numerical methods*

Abstract *This study evaluates low Reynolds number models of turbulence for numerical computations on the heat transfer and fluid flow behavior in a rectangular channel with streamwise-periodic ribs mounted on one of the principal walls. The models include $k-\tilde{\varepsilon}$ models of Launder and Sharma (1974), Chien (1982), $k-\tilde{\varepsilon}$ model of Lin and Hwang (1998), Wilcox's $k-\omega$ model (Wilcox, 1994) and Durbin's model $k-\varepsilon-v^2$ (Durbin, 1995). The numerical results show that all these models can predict the flowfield reasonably well, and the inclusion of the Yap term (Yap, 1987) in the ε – equation (or $\tilde{\varepsilon}$ – equation) can further improve the prediction in these $k-\varepsilon$ models, $k-\tilde{\varepsilon}$ model and $k-\varepsilon-v^2$ model. However, these models behave differently in heat transfer computations. The $k-\omega$ model leads to too low a level of heat transfer and turbulence. Among these $k-\varepsilon$ models and the $k-\tilde{\varepsilon}$ model, Lin's model with the Yap term predicts the heat transfer level best. Durbin's model with extra $\overline{v^2}, f$ equations and the Yap term exhibits further improvement.*

Nomenclature

D_e = hydraulic diameter
h = rib height
H = channel height
k = turbulent kinetic energy
Nu = local Nusselt number
P = pressure
$\hat{P}$ = reduced pressure
Pi = rib pitch
PR = rib pitch-to-rib height ratio, Pi/h
Pr = Prandtl number
$\mathrm{Pr_t}$ = turbulent Prandtl number
Re = Reynolds number, $\mathrm{Re} = \frac{\rho U_{ref} D_e}{\mu}$
T = temperature
$\hat{T}$ = reduced temperature
t = time
U = axial mean velocity
V = transverse mean velocity
w = rib width
x = axial coordinate
y = transverse coordinate
β = pressure drop per pitch
γ = temperature gradient across one pitch
ε = dissipation rate of turbulent kinetic energy
ω = dissipation per unit turbulent kinetic energy
μ = molecular dynamic viscosity
μ_t = turbulent dynamic viscosity
υ = kinetic viscosity
δ_{ij} = Kronecker delta function
$\mathrm{y^+}$ = normalized y coordinate, $\frac{\rho y U_\tau}{\mu}$
y_λ = Taylor microscale $\sqrt{\frac{\upsilon k}{\tilde{\varepsilon}}}$

The authors would like to thank the National Science Council of the Republic of China for its support under contract NSC-85-00413-E007-051.

Introduction

Repeated rib-turbulators in flow passage at periodic intervals can enhance the removal of heat transfer for many engineering applications. The flow separation zones ahead and after the ribs generate secondary motion across the passage so that the turbulence and heat transfer levels increase significantly. Computations of flow and heat transfer through ribbed passage need appropriate turbulence models and most of the computations employed high-Re models of turbulence with the wall function approach. However, the anisotropy of near wall turbulence and the secondary motion across the wall sub-layer make the wall function approach inappropriate. Fewer works (Fusegi, 1996; Iacovides and Raisee, 1997; Taylor *et al.*, 1991) have employed variants of low Reynolds number models of turbulence and suggested the need for tests for more refined low-Re models. $k-\varepsilon$ and $k-\omega$ models are the most popular models for turbulence computation, but most low-Re versions of turbulence models are developed and evaluated for flows through smooth passages. Applicability of these models for ribbed passages needs to be evaluated.

There are numerous versions of $k-\varepsilon$ turbulent models in the low Reynolds number form. According to the evaluations by Patel *et al.* (1985) for two-equation turbulence models in low Reynolds number form, the tests with a variety of boundary layer flows show that the $k-\varepsilon$ models of Launder and Sharma (1974), Chien (1982) and Lam and Bremhorst (1981), and the $k-\omega$ model of Wilcox and Rubesin (1980) were found to be considerably better than the other four models. Therefore, widely used $k-\varepsilon$ models of Launder and Sharma (1974), Chien (1982), and the $k-\omega$ model of Wilcox and Rubesin (1980) are selected for the present study. In addition to these models, the refined $k-\tilde{\varepsilon}$ model of Lin (1998) and $k-\varepsilon-v^2$ model of Durbin (1995) have been newly developed with special considerations in the near wall region. Their models demonstrate excellent improvements on various applications. For example, fully developed plane Couette-Poiseuille flow and backward-facing flow by Lin's model (Lin, 1998), and turbulent separated flows over a back step in a plane diffuser and around a triangular cylinder by Durbin's $k-\varepsilon-v^2$ model (Durbin, 1995). It is worth applying it to the ribbed passage and checking if any improvements can be made.

The present work intends to compare the predictions by above mentioned low-Re turbulence models in four categories:

(1) well-known models of Launder and Sharma (1974) and Chien (1982);

(2) Wilcox's $k-\omega$ model (Yang *et al.*, 1995);

(3) recently developed $k-\tilde{\varepsilon}$ model of Lin (1998); and

(4) $k-\varepsilon-v^2$ model of Durbin (1995).

Modification of the above models is also implemented, i.e. the addition of a correction term to the ε-equation ($\tilde{\varepsilon}$-equation) (Yap, 1987) to eliminate the excessively high levels of near wall turbulence by most turbulence models.

In this paper, numerical computations on the heat transfer and fluid flow behaviour in a rectangular channel with streamwise-periodic ribs mounted on one of the principal walls are performed based on the flow measurements by Drain and Martin (1985) and heat transfer measurements by Liou *et al.* (1993). In order to overcome the difficulty to achieve convergence in complex turbulent flow computation with these turbulence models, the present work applies an efficient Bi-CGSTAB algorithm (van der Vost, 1992) to solve the matrix systems to reach stable and robust convergence (Tsai *et al.*, 1997) so that the performance of these models can be demonstrated by comparing the measurements and numerical predictions.

Governing equations

Measurements reported that the flow pattern reached fully developed after several ribs, for example, 29 ribs in Drain and Martin's work (1985), ten ribs in Chang's work (1990). Since there were 17-19 ribs included in Liou's work (1993), periodic fully developed condition is assumed and the simulation can be simplified by solving the time-dependent, Reynolds-averaged, incompressible Navier-Stokes equations for periodic fully developed turbulent flow. The equations in Cartesian tensor notation can be written as follows:

Continuity equation

$$\frac{\partial U_i}{\partial x_j} = 0$$

Momentum equations

$$\frac{\partial(\rho U_i)}{\partial t} + \frac{\partial \rho U_i U_j}{\partial x_j} = \beta\delta_{il} - \frac{\partial \hat{P}}{\partial x_j} + \frac{\partial}{\partial x_j}[\mu(\frac{\partial U_i}{\partial x_j} + \frac{\partial U_j}{\partial x_i}) - \rho\overline{u_i u_j}]$$

The Reynolds stress can be approximated by adopting Boissinesq approximation within the framework of eddy viscosity:

$$-\rho\overline{u_i u_j} = \mu_t(\frac{\partial U_i}{\partial x_j} + \frac{\partial U_j}{\partial x_i}) - \frac{2}{3}\delta_{ij}k$$

where μ is the molecular viscosity and μ_t is the turbulent viscosity.

In the fully developed region, the pressure drop per pitch is a constant (β), i.e. $P(x + Pi, y) = P(x, y) - \beta \cdot Pi$, where Pi is the pitch length. If we define $\hat{P}(x, y) = \beta x + P(x, y)$ then we have the following relations:

$$\hat{P}(x + n \cdot Pi, y) = \hat{P}(x + (n-1) \cdot Pi, y) = \cdots = \hat{P}(x, y)$$

where n is an integer and $\hat{P}$ repeats itself from pitch to pitch.

Energy equation

$$\frac{\partial(\rho\hat{T})}{\partial t}+\frac{\partial(\rho U_i\hat{T})}{\partial x_i}=\frac{\partial}{\partial x_i}[(\frac{\mu}{\mathrm{Pr}}+\frac{\mu_i}{\mathrm{Pr}_t})\frac{\partial\hat{T}}{\partial x_i}]-\rho U_i\gamma\delta_{il}$$

where Pr is the Prandtl number, Pr_t is the turbulent Prandtl number, δ_{il} is the Kronecker delta function, l is the streamwise direction, $\hat{T}=T-\gamma x$, and γ is the temperature gradient across one pitch which is defined as

$$\gamma=\frac{T(x+Pi,y)-T(x,y)}{Pi}$$

Turbulence models in low-Reynolds number form

Brief descriptions of the transport equations of turbulent properties for various models are given as follows:

$k-\varepsilon$ model

$$\frac{\partial(\rho k)}{\partial t}+\frac{\partial(\rho U_j k)}{\partial x_j}=\frac{\partial}{\partial x_j}[(\mu+\frac{\mu_t}{\sigma_k})\frac{\partial k}{\partial x_j}]-\rho\overline{u_iu_j}\frac{\partial U_i}{\partial x_j}-\rho(\bar{\varepsilon}+D)$$

$$\frac{\partial(\rho\bar{\varepsilon})}{\partial t}+\frac{\partial(\rho U_j\bar{\varepsilon})}{\partial x_j}=\frac{\partial}{\partial x_j}[(\mu+\frac{\mu_t}{\sigma_\varepsilon})\frac{\partial\bar{\varepsilon}}{\partial x_j}]-\rho C_{\bar{\varepsilon}1}f_1\frac{\bar{\varepsilon}}{k}\overline{u_iu_j}\frac{\partial U_i}{\partial x_j}$$

$$-\rho C_{\bar{\varepsilon}2}f_2\frac{\bar{\varepsilon}^2}{k}+E\quad \mu_t=\rho C_\mu f_\mu\frac{k^2}{\bar{\varepsilon}}$$

The constants and damping functions for the models of Launder and Sharma (1974) and Chien (1982) in the above equations are listed in Table I, and $\bar{\varepsilon}$ is the

Code	LS	CH
C_μ	0.09	0.09
f_μ	$\exp(-\frac{3.4}{(1+0.02R_t)^2})$	$1-\exp(-0.0115y^+)$
σ_k	1.0	1.0
$\sigma_{\bar{\varepsilon}}$	1.3	1.3
D	$2\upsilon(\frac{\partial\sqrt{k}}{\partial y})^2$	$2\upsilon\frac{k}{y^2}$
E	$2\upsilon\upsilon_t(\frac{\partial^2U_i}{\partial x_j\partial x_k})^2$	$-2\upsilon(\frac{\bar{\varepsilon}}{y^2})\exp(-0.5y^+)$
f_1	1	1
f_2	$1-0.3\exp(-R_t^2)$	$1-0.22\cdot\exp(-\frac{R_t^2}{36})$
$C_{\bar{\varepsilon}1}$	1.44	1.35
$C_{\bar{\varepsilon}2}$	1.92	1.8
R_t	$\frac{k^2}{\upsilon\bar{\varepsilon}}$	$\frac{k^2}{\upsilon\bar{\varepsilon}}$
		$y^+=\frac{yU_\tau}{\upsilon}$

Table I.
Constants and damping functions for Launder and Sharma's (1974) and Chien's (1982) models

dependent variable of the transport equation. The extra term, denoted by E, makes the value of dissipation rate at wall zero. The $k-\varepsilon$ models of Launder and Sharma (1964) and Chien (1982) are well-known models and there is no need to describe them here.

Lin's $k-\tilde{\varepsilon}$ model

$$\frac{\partial(\rho k)}{\partial t}+\frac{\partial(\rho U_j k)}{\partial x_j}=\frac{\partial}{\partial x_j}[(\mu+\frac{\mu_t}{\sigma_k})\frac{\partial k}{\partial x_j}]+\Pi_k-\rho\overline{u_i u_j}\frac{\partial U_i}{\partial x_j}-\rho(\tilde{\varepsilon}+\hat{\varepsilon})$$

$$\frac{\partial(\rho\tilde{\varepsilon})}{\partial t}+\frac{\partial(\rho U_j\tilde{\varepsilon})}{\partial x_j}=\frac{\partial}{\partial x_j}[(\mu+\frac{\mu_t}{\sigma_\varepsilon})\frac{\partial\tilde{\varepsilon}}{\partial x_j}]+\Pi_{\tilde{\varepsilon}}-\rho C_{\tilde{\varepsilon}}\, f_1\frac{\tilde{\varepsilon}}{k}\overline{u_i u_j}\frac{\partial U_i}{\partial x_j}$$

$$-\rho C_{\tilde{\varepsilon}2}\, f_2\frac{\tilde{\varepsilon}^2}{k}\mu_t=\rho C_\mu\, f_\mu\frac{k^2}{\tilde{\varepsilon}}$$

where

$$C_\mu=0.09,\sigma_k=1.4-1.1\cdot\exp(-\frac{y_\lambda}{10}),\sigma_{\tilde{\varepsilon}}=1.3-\exp(-\frac{y_\lambda}{10}),$$

$$C_{\tilde{\varepsilon}1}=1.44,C_{\tilde{\varepsilon}2}=1.92,\ y_\lambda=\frac{y\sqrt{\tilde{\varepsilon}}}{\sqrt{\upsilon k}},\ f_\mu=1-\exp(-\frac{y_\lambda}{100}-\frac{8y_\lambda^3}{1,000}),$$

$$\Pi_k=-\frac{1}{2}\frac{\partial}{\partial x_j}(\mu\frac{k}{\varepsilon}\frac{\partial\hat{\varepsilon}}{\partial x_j}),\ \Pi_{\tilde{\varepsilon}}=-\frac{\partial}{\partial x_j}(\mu\frac{\tilde{\varepsilon}}{k}\frac{\partial k}{\partial x_j}),\ \hat{\varepsilon}=2\upsilon(\frac{\partial\sqrt{k}}{\partial y})^2,$$

$$f_1=1,\ f_2=1-0.22\cdot\exp(-\frac{R_t^2}{36}),\ R_t=\frac{k^2}{\upsilon\tilde{\varepsilon}}.$$

Comparing Lin's $k-\tilde{\varepsilon}$ model with previous $k-\varepsilon$ models, the differences are:

(1) including pressure diffusion term Π_k in the k-equation and extra term in $\tilde{\varepsilon}$-equation;

(2) using $\tilde{\varepsilon}$ as the dependent variable of the transport equation instead of ε, ε is the dissipation rate of turbulent energy which can be decomposed into two parts, i.e. $\varepsilon=\tilde{\varepsilon}+\hat{\varepsilon}$;

(3) adopting the Taylor microscale (Tennekes and Lumley, 1972) of y_λ in the damping functions.

The adopted form of f_μ reproduces correctly the asymptotic limit towards the wall and avoids the singularity occurring at the reattachment point by adopting y^+.

The justifications of the use of Lin's model are given in the following paragraph.

Moin's DNS data (Moin *et al.*, 1988) indicates that $\frac{\partial\varepsilon}{\partial y}<0$ at the wall, and this shows that the maximum value of ε should be located at the wall. These

necessitate the inclusion of the pressure diffusion term Π_k in the k-equation, especially in the near wall region.

The inclusion of $\Pi_{\tilde{\varepsilon}}$ in $\tilde{\varepsilon}$-equation is to balance the molecular diffusion at the wall. This idea was also adopted by Chien (1982) and Kawamura (1991), but with different formulation. Lin's formulation mimics the diffusive nature of the pressure diffusion term. Furthermore, $\Pi_{\tilde{\varepsilon}}$ also generate the extra source for ε in the buffer zone, and the commonly adopted format $\frac{\mu\mu_t}{\rho}(\frac{\partial U_i}{\partial x_j \partial x_k})^2$ was completely replaced.

Therefore, Lin claimed that his model not only conforms with the near wall characteristics obtained with the direct numerical simulation data but also possesses the correct asymptotic behavior in the vicinity of the wall. The application of Lin's model produced correctly the skin friction and near wall heat transfer coefficient for a two-dimensional backward-facing step (Lin, 1998).

Wilcox's $k = \omega$ model

$$\frac{\partial(\rho k)}{\partial t} + \frac{\partial(\rho U_j k)}{\partial x_j} = \frac{\partial}{\partial x_j}[(\mu + \sigma^* \mu_t)\frac{\partial k}{\partial x_j}] + \rho(P_k + D_k)$$

$$\frac{\partial(\rho \omega)}{\partial t} + \frac{\partial(\rho U_j \omega)}{\partial x_j} = \frac{\partial}{\partial x_j}[(\mu + \sigma \mu_t)\frac{\partial \omega}{\partial x_j}] + \rho(D_\omega + P_\omega + C_\omega)$$

$$\mu_t = \rho \alpha^* \frac{k}{\omega}$$

where

$$P_k = \alpha^* \frac{k}{\omega}\Omega^2,\ D_k = -B^* \omega k,\ P_\omega = \alpha \alpha^* \Omega^2,$$

$$C_\omega = \max\{0, \frac{\sigma_d}{\omega}(\frac{\partial k}{\partial x}\frac{\partial \omega}{\partial x} + \frac{\partial k}{\partial y}\frac{\partial \omega}{\partial y})\},\ D_\omega = -B\omega^2$$

$$\sigma^* = 1, \sigma = 0.6,\ R_k = 6,\ R_\beta = 8,\ R_\omega = 2.2, \alpha_0^* = 0.025, \sigma_d = 0.3$$

$$\mathrm{Re}_t = \frac{\rho}{\mu}\frac{k}{\omega},\ a^* = \frac{R_k \alpha_0^* + \mathrm{Re}_t}{R_k + \mathrm{Re}_t},\ \alpha = \frac{1}{2}\frac{R_\omega \alpha_0 + \mathrm{Re}_t}{(r_\omega + \mathrm{Re}_t)\alpha^*},\ \alpha_0 = 0.1,$$

$$B = 0.075,\ B^* = 0.09 + \frac{\frac{5}{18} + (\frac{\mathrm{Re}_t}{R_\beta})^4}{1 + (\frac{\mathrm{Re}_t}{R_\beta})^4},\ \Omega^2 = (\frac{\partial u}{\partial y} + \frac{\partial v}{\partial x})^2 + 2[(\frac{\partial u}{\partial x})^2 + (\frac{\partial v}{\partial y})^2].$$

This model is widely used and the details can be referenced in Wilcox's work (Wilcox and Rubensin, 1980; Wilcox, 1993a, 1993b, 1993c, 1994).

Durbin's $k = \varepsilon - v^2$ model

$$\frac{\partial(\rho k)}{\partial t} + \frac{\partial(\rho U_j k)}{\partial x_j} = \frac{\partial}{\partial x_j}[(\mu + \frac{\mu_t}{\sigma_k})\frac{\partial k}{\partial x_j}] + P_k - \rho\varepsilon$$

$$\frac{\partial(\rho\varepsilon)}{\partial t} + \frac{\partial(\rho U_j \varepsilon)}{\partial x_j} = \frac{\partial}{\partial x_j}[(\mu + \frac{\mu_t}{\sigma_\varepsilon})\frac{\partial \varepsilon}{\partial x_j}] + \frac{\rho C_{\varepsilon 1} P_k - \rho C_{\varepsilon 2}\varepsilon}{T}$$

$$\frac{\partial(\rho\overline{v^2})}{\partial t} + \frac{\partial(\rho U_j \overline{v^2})}{\partial x_j} = \frac{\partial}{\partial x_j}[(\mu + \frac{\mu_t}{\sigma_k})\frac{\partial \overline{v^2}}{\partial x_j}] + \rho k f - \rho\overline{v^2}\frac{\varepsilon}{k}$$

$$L^2\nabla^2 f - f = (1 - C_1)\frac{[\frac{2}{3} - \frac{\overline{v^2}}{k}]}{T} - C_2\frac{P_k}{k},$$

$$\mu_t = \rho C_\mu \overline{v^2} T.$$

where

$$\sigma_k = 1.0, \sigma_\varepsilon = 1.3, C_{\varepsilon 1} = 1.3 + \frac{0.25}{1 + (\frac{d}{2\ell})^8},$$

$$C_{\varepsilon 2} = 1.9, C_\mu = 0.19, C_L = 0.3, C_\eta = 70,$$

$$\ell = \frac{L}{C_L}, C_1 = 1.4, C_2 = 0.3, \mathrm{d} : \text{distance to the closest boundary},$$

$$L = C_L \max(\frac{k^{1.5}}{\varepsilon}, C_\eta(\frac{\upsilon^3}{\varepsilon})^{\frac{1}{4}}), T = \max(\frac{k}{\varepsilon}, 6(\frac{\upsilon}{\varepsilon})^{\frac{1}{2}}).$$

Durbin's $k - \varepsilon - v^2$ model (Durbin, 1995) is proposed for computing non-equilibrium, or complex, turbulent flows. In his model, the velocity scale for turbulent transport towards the wall is $\overline{v^2}$, not k. Extra two parameters $\overline{v^2}$ and f, need to be solved via $\overline{v^2}$ transport equation and elliptic relaxation equations for f. The variable $\overline{v^2}$ is a velocity scale and might loosely be regarded as the velocity fluctuation normal to the streamlines. Also, $\overline{v^2}$ behaves as the wall normal component of turbulent intensity near the surfaces. Impermeable boundaries cause non-local suppression of $\overline{v^2}$, and the elliptic relaxation equation for f is the mathematical representation of non-locality. It is designed to use in wall-bounded flows. Good agreement between experiment and predictions are obtained for turbulent separated flows over a backward-facing step, in a plane diffuser, and around a triangular cylinder, and jet impinging onto a pedestal using a revised model (Durbin *et al.*, 1997).

Yap term

It is well-known that the energy dissipation equation of turbulence models, in particular the low Reynolds number $k - \varepsilon$ model, produces too large a turbulence length scale for separated flows. Therefore, excessively high levels of near-wall turbulence and heat transfer are obtained. Yap (1987) introduced a term into the ε-equation (or $\tilde{\varepsilon}$-equation) to reduce the departure from the local-

equilibrium length scale in wall turbulence. The correction term YC, namely the Yap term, is expressed as

$$YC = \max\{0.83\frac{\rho\varepsilon^2}{\mathrm{k}}(\frac{k^{1.5}}{\varepsilon}\frac{1}{2.55Y} - 1)(\frac{k^{1.5}}{\varepsilon}\frac{1}{2.55Y})^2, 0\}$$

where Y is the distance to the closest walls. This Yap term is added to the ε-equation (or $\tilde{\varepsilon}$-equation) for the above $k-\varepsilon$ turbulence models or $\tilde{\varepsilon}$-equation for Lin's model, so that better predictions on flow and heat transfer characteristics can be expected.

Boundary conditions

At the inlet and outlet of the calculated flow domain, the periodic behaviour leads to the periodic boundary conditions for the applied turbulence models, i.e.

$$U_i(0,y) = U_i(Pi,y), \quad k(0,y) = k(Pi,y), \quad \varepsilon(0,y) = \varepsilon(Pi,y)$$
$$\tilde{\varepsilon}(0,y) = \tilde{\varepsilon}(Pi,y), \quad \hat{P}(0,y) = \hat{P}(Pi,y), \quad \hat{T}(0,y) = \hat{T}(Pi,y),$$
$$\bar{\varepsilon}(0,y) = \bar{\varepsilon}(Pi,y).$$

At all surfaces of the ribs and the walls of the flow channel, no-slip boundary condition is applied and the turbulent kinetic energy k is set to zero. For the models of Launder and Sharma (1974), Chien (1982) and Lin (1998), $\bar{\varepsilon}$ or $\tilde{\varepsilon}$ is set to zero at wall boundaries. As for Durbin's model, periodic boundary conditions are applied on variables of $\varepsilon, \overline{v^2}$ and f at the inlet and outlet of the flow channel, zero is assigned for $\overline{v^2}, f, k$ at the solid walls, and ε is evaluated by the equation

$$\varepsilon(y) = \frac{2\mu}{\rho}\frac{\mathrm{k}}{\mathrm{y}^2}$$

as y approaches zero. For the $k-\omega$ model, periodic boundary condition is also applied for ω, and the asymptotic equation of $\omega(y) \to \frac{2\mu}{B^*\rho y^2}$ as $y \to 0$ is applied near the solid wall.

Numerical methods

The governing equations are discretized in finite volume approach with staggered grid arrangement. At each control volume, the difference equations can be expressed as

$$[\mathrm{A}_\mathrm{p}^* + \frac{\rho\ \mathrm{vol}}{\Delta\mathrm{t}}]\phi_\mathrm{p}^{n+1} = AE\phi_\mathrm{p}^{n+1} + AW\phi_\mathrm{p}^{n+1} + AN\phi_\mathrm{p}^{n+1} + AS\phi_\mathrm{s}^{n+1} + b_\phi + \frac{\rho\mathrm{vol}}{\Delta\mathrm{t}}\phi_\mathrm{p}^{\mathrm{n}}$$

where the subscript P indicates the Pth control volume, E represents the node located at the East of the Pth node, and W, N, S nodes are located next to P node at the West, North, and South directions respectively, $A_p^* = AE + AW + AN + AS$ and the coefficients $AE \geq 0, AW \geq 0, AN \geq 0, AS \geq 0$ are convective and

diffusion terms handling by the hybrid scheme (Patankar, 1980). The difference equations can be arranged into a linear system $A\phi = b$, where A is usually a non-symmetric, penta-diagonal matrix.

This linear system $A\phi = b$ can be solved by Gauss-Seidel iterative method, but the rate of convergence is slow. In order to achieve fast convergence, the Bi-CGSTAB method (van der Vost, 1992) is employed in our study.

Since the convergence rate of CG methods strongly depends on the eigenvalue distribution of the coefficient matrix A, it is desirable to redistribute the eigenvalue distribution by the application of preconditioned technique. That is, we can find a matrix M, namely preconditioner, such that the eigenvalues of $M^{-1}A$ are a more clustered unitary, and the alternative system $M^{-1}A\phi = M^{-1}b$ instead of the original system $A\phi = b$ is solved. Modified ILU is chosen as the preconditioner in our study, i.e. $M = \hat{L}\hat{U}$ which is the incomplete lower and upper factorization of the matrix A, $\hat{L}$ is a sparse lower triangular matrix and $\hat{U}$ is a sparse upper triangular matrix.

In our study, the PISO algorithm (Issa, 1985) is employed to couple the velocities and pressure in the governing equations, and Bi-CGSTAB method (van der Vost, 1992) is employed to solve the alternative system $M^{-1}A\phi = M^{-1}b$. This numerical method had demonstrated fast and stable convergence in computations for cases of turbulent separation flows (Tsai *et al.*, 1997).

The preconditioned Bi-CGSTAB algorithm for solving $M^{-1}A\phi = M^{-1}b$ is described in the following.

Preconditioned Bi-CGSTAB Algorithm: (solve $M^{-1}Ax = M^{-1}b$)

Give x_0 and $r_0 = b - Ax_0$
Choose $\hat{r}_0 = M{-}1r_0$
$\rho_0 = \alpha = \omega_0 = 1, v_0 = p_0 = 0$

For i = 1, 2, 3, . . .
$\rho_i = (\hat{r}_0, r_{i-1})$
$\beta = \dfrac{\rho_i}{\rho_{i-1}} \dfrac{\alpha}{\omega_{i-1}}$
$p_i = r_{i-1} + \beta(p_{i-1} - \omega_{i-1}v_{i-1})$
solve y from $My = p_i$
$v_i = Ay$
$\alpha = \dfrac{\rho}{(\hat{r}_0, v_i)}$
$s = r_{i-1} - \alpha v_i$
solve Z from $Mz = s$
$t = Az$
$\omega_i = \dfrac{(t, s)}{(t, t)}$
$x_i = x_{i-1} + \alpha y + \omega_i z$

If x_i is accurate enough then stop
$r_i = s - \omega_i t$
i = i + 1
End for

Results and discussion

The computed fluid mean flow profiles are compared with the measurement of Drain and Martin (1985) who performed Laser-Doppler velocimetry (LDV) measurements of fully developed water flow in a rectangular duct with one surface roughened by a periodic rib structure. The Reynolds number based on the channel height is 3.72×10^4, the ratio of rib and channel height is 0.2 (h/H = 0.2), and the rib pitch-to-rib height ratio (PR = Pi/h) is 7.2. Figure 1(a) plots the ribbed channel geometry and the calculation domain. Since the passage is long enough for repeating flow conditions to prevail over each rib interval, the numerical flow domain covers only one rib interval and periodic flow boundary conditions are applied. The results predicted here are obtained using 107×126 grid system, in which the first grid nodes next to the wall were placed at $y^+ \leq 0.3$ (where $y^+ = \frac{\rho y U_\tau}{\mu}$ is the normalized y coordinate).

Velocity profiles

For this problem, the separation bubble downstream of the rib extends over almost half the rib interval and a smaller bubble exists ahead of the rib. Figure 1(b) illustrates the physical coordinate system along the ribbed wall for the following figures. Figure 2(a) compares the measured mean velocity profiles with the computed profiles by Launder and Sharma's model. The computations obtain the main feature of the flow field with somewhat different sizes of separation bubble ahead of the rib (s > 0) and thicker boundary layers on the top surface of the rib (s/h > 7.2). In this Figure, four profiles of streamwise velocity distribution are shown, namely, s/h = 3.18, s/h = 4.32, s/h = 7.3, and s/h = 7.7 respectively, where the positions at s/h = 7.3 and s/h = 7.7 are located above the rib. This Figure shows that the mean velocity profiles agree well worth the experimental data at most of the height levels, y/H, except near the

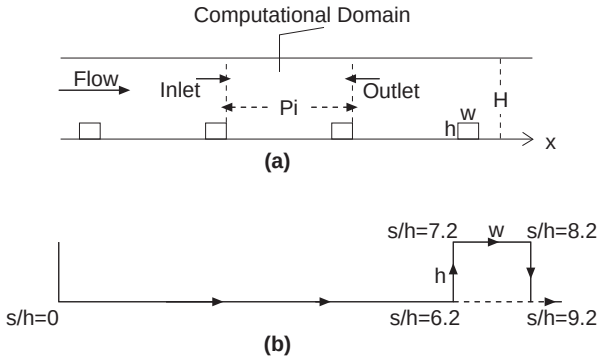

Figure 1.
(a) sketch of computational domain; (b) coordinate system along the principal wall (w = h, H/h = 5, PR = Pi/h = 7.2)

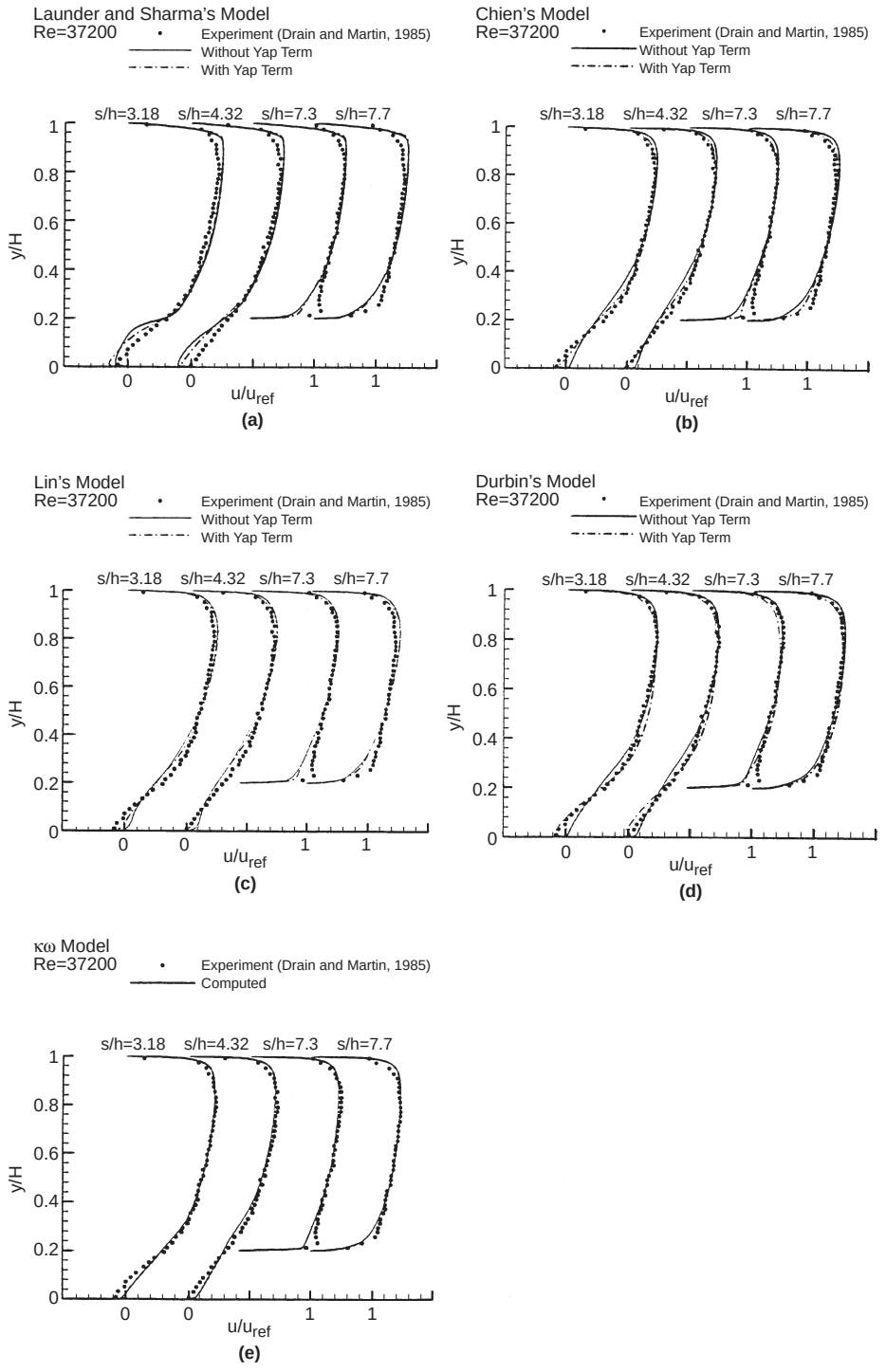

Figure 2.
Streamwise velocity profiles using (a) Launder and Sharma's model; (b) Chien's model; (c) Lin's model; (d) Durbin's model; (e) Wilcox's $k - \omega$ model

surface wall. For this case, the reattachment point occurrs approximately at s/h ≒ 4.32, and the computed separation bubble is larger than the measured one. Moreover, at s/h = 7.3, the computed boundary layer is thicker than the measured layer. Figure 2(a) also shows that the addition of the the Yap term in the ε-equation improves the prediction of the reversed flow field using Launder and Sharma's model. Figure 2(b) plots the flow field obtained by Chien's model. Differing from the previous model, a smaller separation bubble is obtained in this model. Similar to the model of Launder and Sharma, computed boundary layer on the top of the rib is thicker than the measured value. Again, the addition of the Yap term in the ε-equation improves the prediction of the velocity profile at all four stations. As Lin's model is applied, a smaller separation bubble than the measured one is also observed as the velocity profiles at s/h = 3.18, s/h = 4.32 indicate (Figure 2(c)) and slower developments of the velocity profiles on top of the rib surface are shown at s/h = 7.3, s/h = 7.7. There is little difference in velocity distributions by Chien's and Lin's models. Although Lin's model has special treatment to obtain the correct turbulence properties in the vicinity of the wall, only slight change on the velocity profiles is obtained by the addition of the Yap term. Durbin's model predicts the velocity profiles as well as Chien's and Lin's models, although extra terms of $\overline{v^2}$ and f are calculated to evaluate the time averaged properties (Figure 2(d)). Besides, the Yap term is also needed to achieve better prediction as the $k - \varepsilon - \overline{v^2}$ model is used. Wilcox (1993a, 1993b, 1993c, 1994) had performed a series of computations and demonstrated that the $k - \omega$ model was accurate for boundary layers with adverse pressure gradient and suggested the use of the $k - \omega$ model for studying transition and surface roughness effect. In this case, it is found that the predicted profiles at various locations agree well with the measured profiles, and slight improvement is observed compared to those predicted profiles in the above four $k - \varepsilon$ models without the Yap term (Figure 2(e)). Since the Yap term is an additional term in the ε-equation (or $\tilde{\varepsilon}$-equation), the addition of the Yap term in the $k - \omega$ model is not applied. In conclusion, the addition of the Yap term in the models of Launder and Sharma, Chien, Lin, and Durbin improves the velocity computation by enlarging the separation bubble after the rib, and reduces the boundary layer thickness at the top surface of the rib. It implies that adding the Yap term corrects the turbulence length scale near the wall and takes care of the non-local-equilibrium of the flow.

Temperature contours and local Nusselt number distribution

The computed temperature contours and the local Nusselt number distributions are compared with the experiment of Liou *et al.* (1993). They employed the real-time holographic interferometry technique to measure the time-dependent temperature field in the ribbed duct. The computation domain and the grid system are the same as in the previous work. The first grid point next to the wall is located at $y^+ < 0.1$ on Reynolds number of 1.26×104. Figure 3 compares the measured temperature contours with the computed ones by various models. The patterns of temperature contour at regions behind and

ahead of the rib illustrate the overall temperature field and the degree of heat transfer. Comparisons of Figures 3(a) and 3(b) indicate that the addition of the Yap term indeed improves the contour pattern especially the regions behind and ahead of the rib if Launder and Sharma's (LS) model is employed. The contour lines' pattern and their gradient under the line of $\hat{T} = 32$ should be regions of emphasis to evaluate the performance of the models qualitatively. Chien's model without the Yap term predicts temperature contour pattern better at the regions ahead of the rib than the LS model and improves

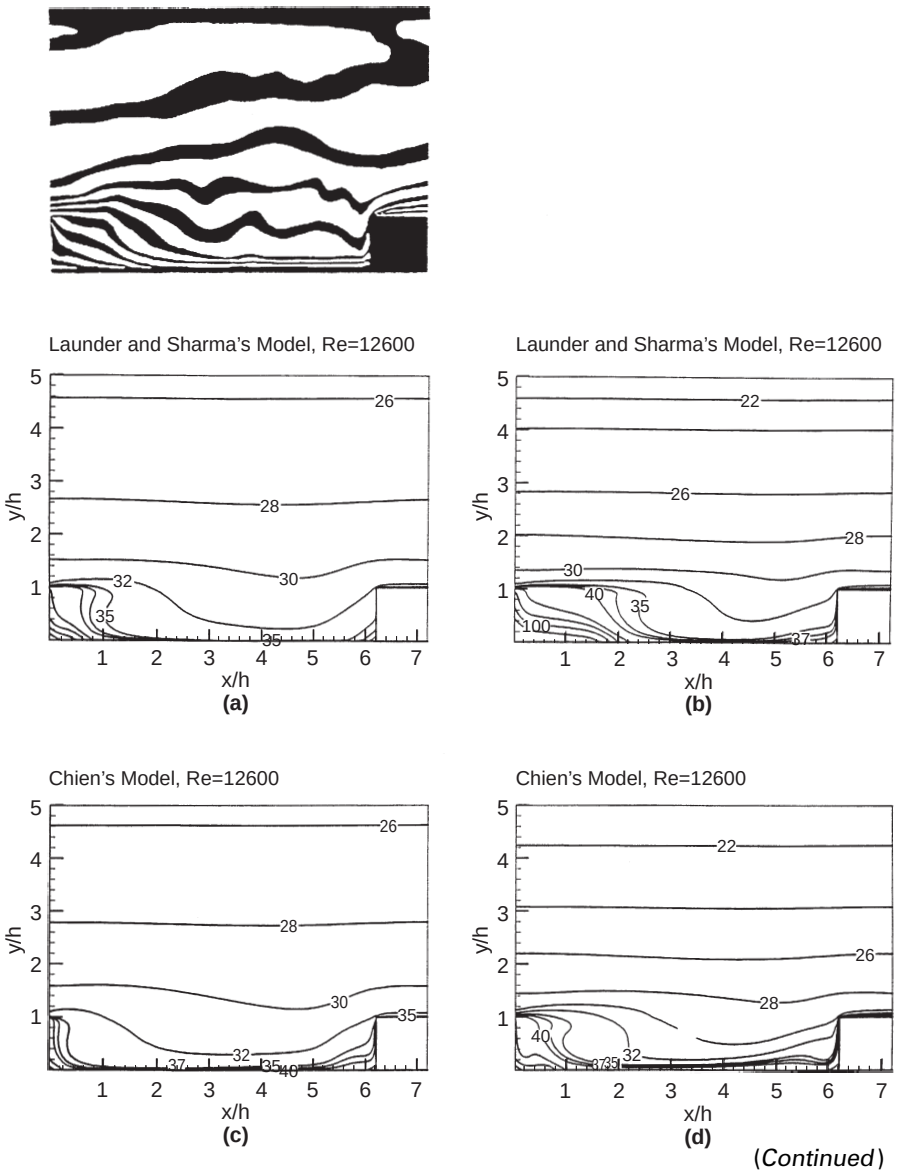

Figure 3.
Reduced temperature contour using (a) Launder and Sharma's model; (b) Launder and Sharma's model with the Yap term; (c) Chien's model; (d) Chien's model with the Yap term (e) Wilcox's $k - \omega$ model; (f) Lin's model; (g) Lin's model with the Yap term; (h) Durbin's $k - \varepsilon - v^2$ model; (i) Durbin's $k - \varepsilon - v^2$ model with the Yap term

(*Continued*)

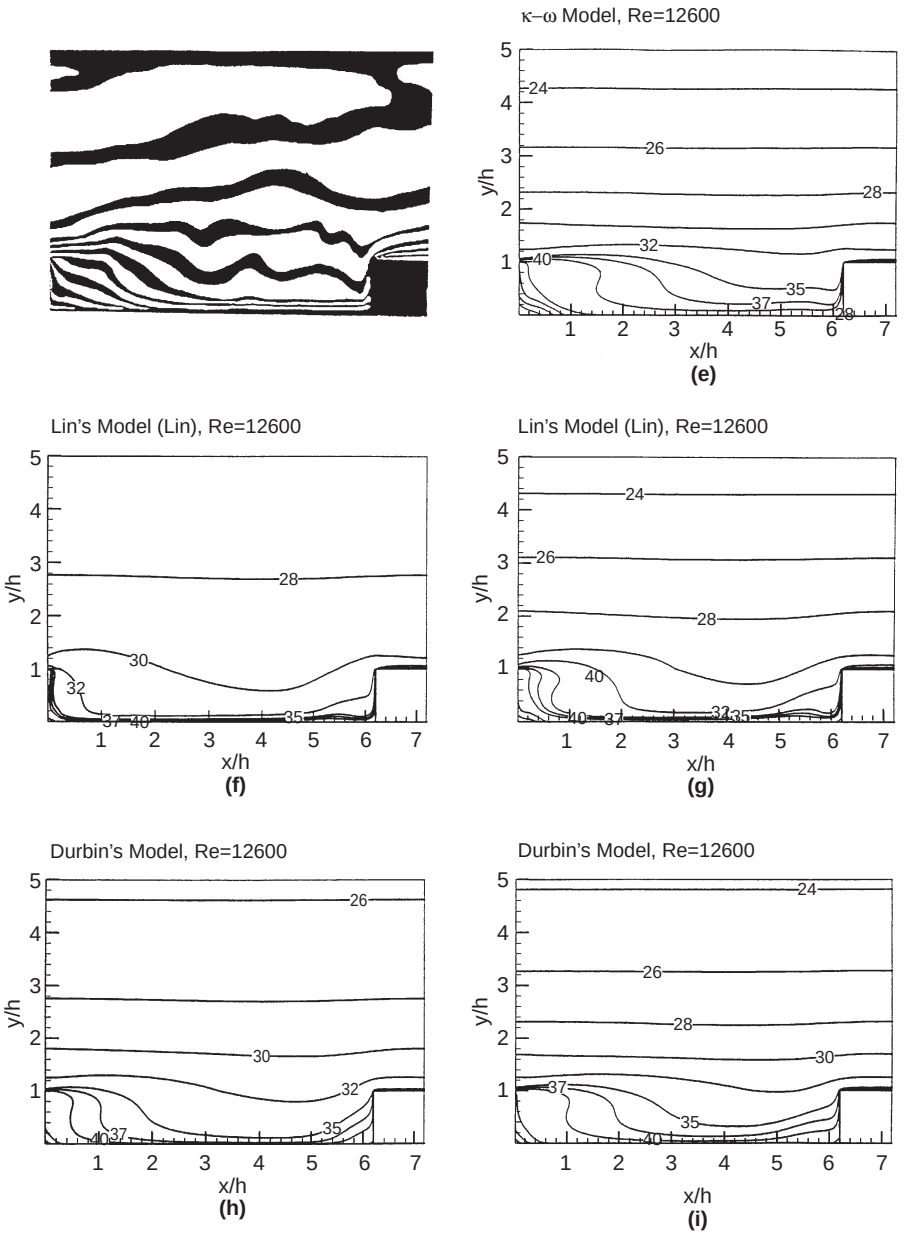

Figure 3

somewhat at the region behind the rib if the Yap term is added. As we compare the contours in Figure 3, Durbin's model and $k-\omega$ give the best matches with measured lines and Lin's model with the Yap term performs reasonably well. Figures 4(a)-4(e) present the measured and computed Nusselt number distributions (where $Nu_s = 0.023\ \mathrm{Re}^{0.8}\ \mathrm{Pr}^{0.4}$) by various turbulence models.

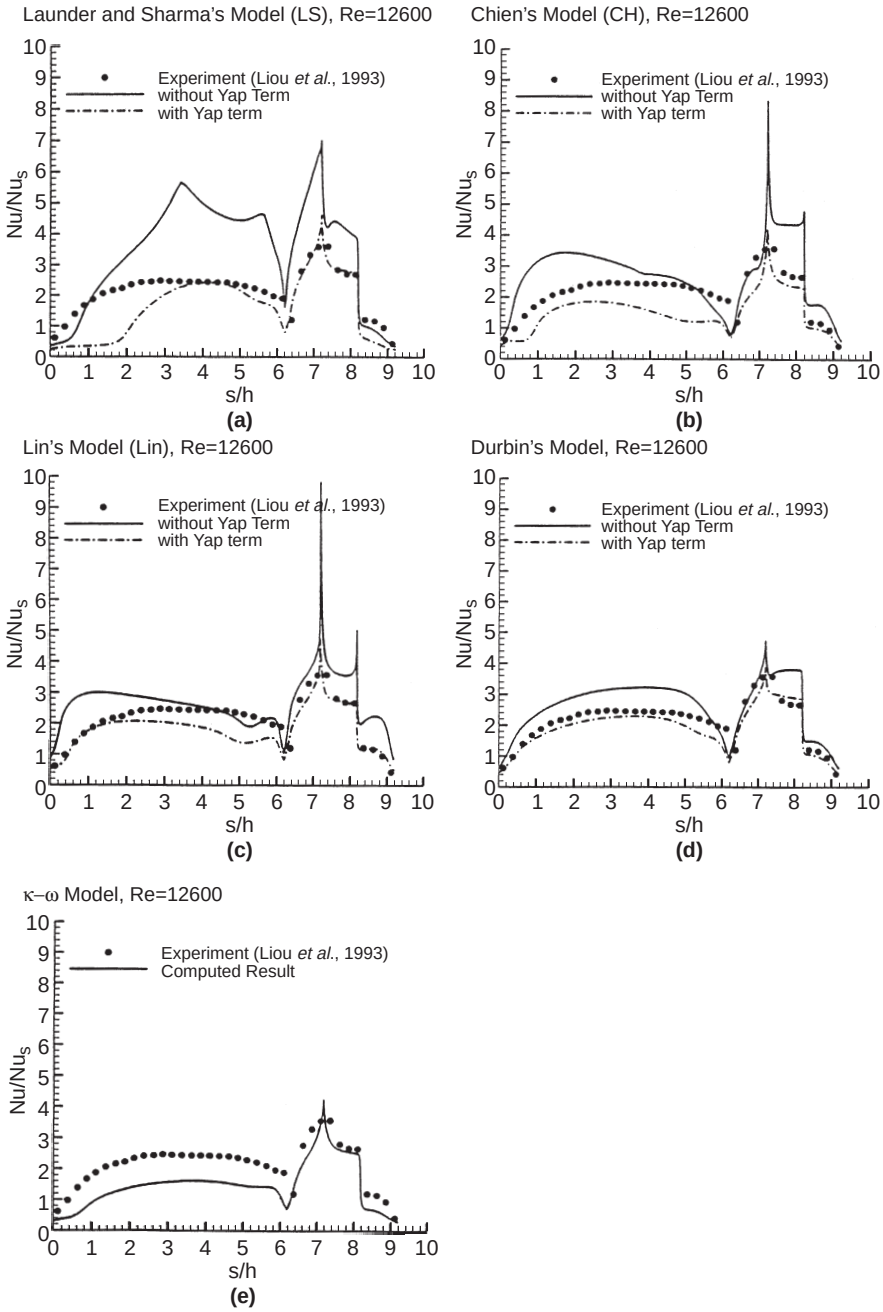

Figure 4.
Local Nusselt number distribution using (a) Launder and Sharma's model; (b) Chien's model; (c) Lin's model; (d) Durbin's model; (e) Wilcox's $k-\omega$ model

Figure 4(a) shows that the model of Launder and Sharma greatly over-predicts the Nusselt number level and the value reaches its maximum too slowly if the Yap term is not included. The level of Nusselt number distribution is lowered

down to the level of measurement in most parts of the axial locations if the Yap term is included. Even with the Yap term, serious discrepancy between the measurement and computation is observed near the upstream corner (s/h = 0), where heat transfer level is seriously underestimated. The same discrepancy occurs at the corner before the rib (s/h = 6.2). However, it is interesting to note that the computed heat transfer coefficient fits well with measured distribution on all surfaces of the rib if LS model when the Yap term is employed. The predicated Nusselt number level by Chien's model agrees with the measured level but with different shapes if the Yap term is not included (Figure 4b) and it is noted that the maximum value of Nu is reached too early (s/h $\approx$ 1). The predicted level is somewhat lower than the measured level after the flow recirculation zone (s/h $\approx$ 1.6) if the Yap term is employed in this model. The overall Nusselt number distribution pattern along s is agreed fairly with the measurement with some discrepancy. Lin's model obtains the Nusselt number distribution with improvement both in distribution shape and magnitude (Figure 4(c)) except the Nusselt number distribution reaches its maximum too early (s/h $\approx$ 1). This is partly due to the correct near-wall turbulent properties, resulting from the satisfaction of the asymptotic limit in the vicinity of the wall. With Lin's model and the Yap term, the heat transfer level is correctly calculated starting from the upstream corner (s/h = 0), but the level is gradually underestimated as the flow goes more downstream (s/h $\approx$ 2.0); however, the heat transfer coefficient on the rib surface is correctly predicted. With extra parameters of $\overline{v^2}$ and f, Durbin's model obtains the Nusselt number level higher than the measured level along the wall and on the surfaces of the rib without the Yap term in the ε-equation, but the distribution shape is much improved. The prediction of the heat transfer level is reduced to the measured level in most part if the Yap term is appended to the ε-equation (Figure 4(d)). Although the $k-\omega$ model predicts the flowfield well in the case of Re = 37,200, under-prediction of heat transfer level with uniform discrepancy from the measured level is observed downstream of the rib, i.e. s/h = 0 to 6 (Figure 4(e)). Good prediction of the heat transfer level on all faces of the rib is achieved. These Nusselt number distributions using various turbulence models reveal that Durbin's model with the Yap term in ε-equation provides the best simulation in local Nusselt number distribution. Two major conclusions are:

(1) These turbulence models can predict the flowfield well away from the wall surface as shown in Figure 2, but they give large variations of heat transfer predictions. Lin's model is the best among $k-\varepsilon$ models. Durbin's $k-\varepsilon-v^2$ model offers some further improvement, and the $k-\omega$ model does not yield the desired level of heat transfer coefficient.

(2) The addition of the Yap term to the ε-equation reduces the level of heat transfer coefficients by all models; it implies that the correction of the turbulence length scale near the wall depresses the turbulent diffusion and thus the heat transfer process. This phenomenon can be verified by the distributions of turbulent properties.

Turbulent kinetic energy contours

Since the $k-\varepsilon$ models use $\mu_t = \rho C_\mu f_\mu k^2/\bar{\varepsilon}$ as the eddy viscosity, the high values of k in the flowfield lead to high heat transfer predictions. The function of the Yap term in the ε-equation is mainly to reduce the excessive turbulent energy so that the heat transfer level can be reduced. The behaviour of heat transfer computations can be viewed and explained by the contour of turbulent kinetic energy.

Figure 5(a) plots the computed turbulent kinetic energy contours using Launder and Sharma's model. Two points at x/h = 0 and 6.2 with y/H = 0.2 are singular points. The levels of turbulent kinetic energy are greatly reduced especially at the flowfield near the rib and wall as the Yap term is applied (Figure 5(b)). The predictions of near-wall turbulence can be improved by Lin's model and the turbulent kinetic energy is enhanced near the wall surfaces (Figure 5(c)). However, it does not consider the non-equilibrium condition within the flowfield and over-predicts the level with non-smooth pattern, therefore, the inclusion of the Yap term which considers the non-equilibrium phenomena cuts down the turbulent kinetic energy level and smoothes out the distribution (Figure 5(d)). The improving turbulence very close to the wall can explain why Lin's model with the Yap term best predicts the heat transfer coefficient among all $k-\varepsilon$ models employed. Figure 5(e) plots the turbulent kinetic energy contours calculated by Durbin's model; smooth distributions are observed. It may explain the role of $\overline{v^2}, f$ terms. The adoption of the Yap term in ε-equation again reduces the levels of turbulence significantly near the rib and wall surface (Figure 5(f)). The correct distribution of turbulent kinetic energy yields the correct heat transfer level. The computed turbulence using the $k-\omega$ model also shows smooth contours (Figure 5(g)) with levels much lower than levels using $k-\varepsilon$ models without the Yap term. The low level of turbulence leads to a low level of heat transfer.

Conclusions

In this study, various versions of low-Reynolds number turbulence models are evaluated by detailed comparisons of the computed and measured flow and heat transfer characteristics in two-dimensional rectangular channel flow with ribbed passage. All the low-Re models tested exhibit the similar performance on the calculation of core flowfield, but behave very differently on the calculations of heat transfer characteristics.

Lin's model with the Yap term leads to the best prediction on heat transfer level among all $k-\varepsilon$ models tested because his model adopted the Taylor microscale in the damping functions and the inclusion of the pressure diffusion terms in both the k and $\tilde{\varepsilon}$ equations. His modification gives the correct behaviour in the vicinity of the wall. The near-wall treatment of the $\overline{v^2}-f$ system of equation helps Durbin's model perform even better than Lin's model on the calculation of heat transfer. Wilcox's $k-\omega$ model underestimates the heat transfer prediction and needs improvement.

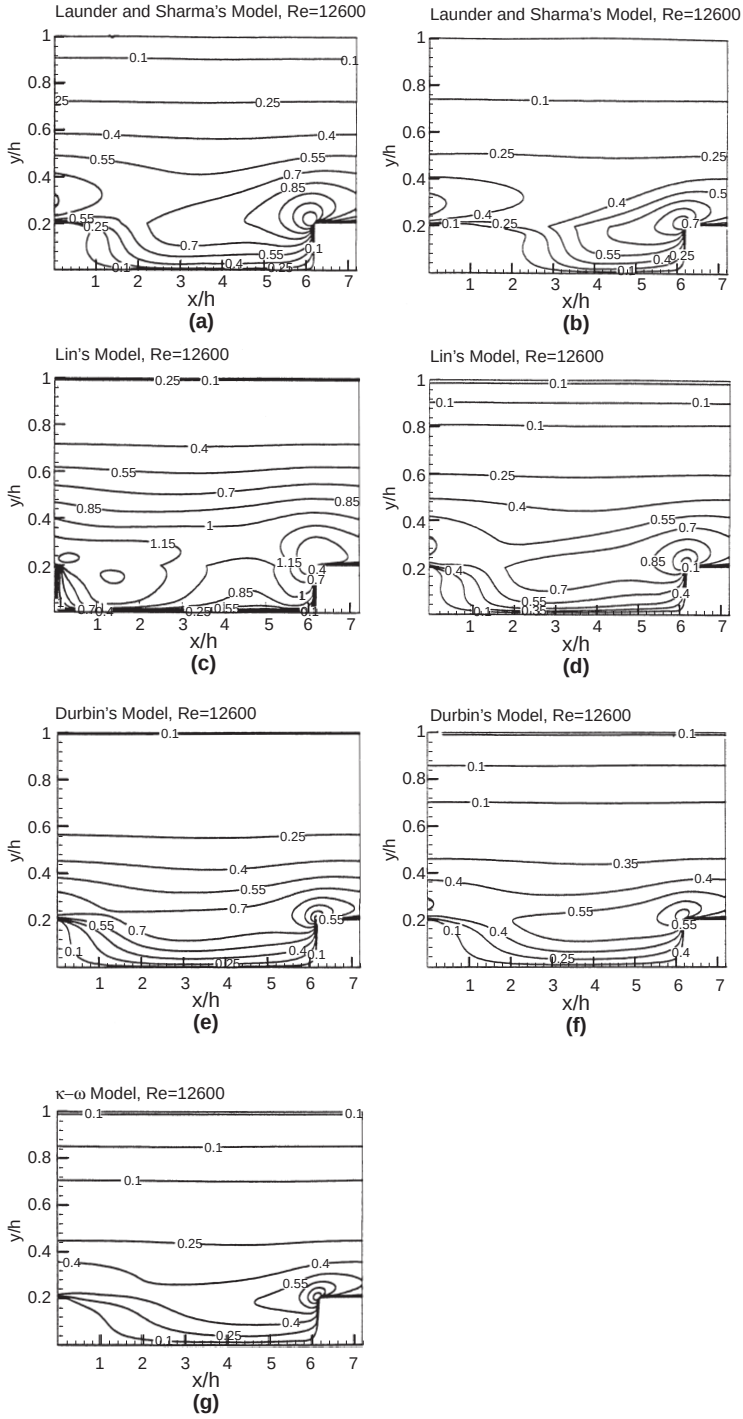

Figure 5.
Turbulent kinetic energy contour:
(a) Launder and Sharma's model without the Yap term;
(b) Launder and Sharma's model with the Yap term;
(c) Lin's model without Yap term;
(d) Lin's model with the Yap term;
(e) Durbin's model without the Yap term;
(f) Durbin's model with the Yap term;
(g) Wilcox's $k - \omega$ model

References

Chang, Y. (1990), "Experimental analysis of turbulent flows in a rectangular duct with repeated square-rib pairs", Master thesis, National Tsing Hua University, Taiwan, ROC.

Chien, K.Y. (1982), "Predictions of channel and boundary-layer flows with a low-Reynolds number turbulence model", *AIAA Journal*, Vol. 20 No. 1, pp. 33-8.

Drain, L.E. and Martin, S. (1985), "Two-component velocity measurements of turbulent flow in a ribbed-wall flow channel", *International Conference on Laser Anemometry – Advances and Application*, Manchester, pp. 99-112.

Durbin, P.A. (1995), "Separated flow computations with the $k - \varepsilon - v^2$ model", *AIAA Journal*, Vol. 33 No. 4, April, pp. 659-64.

Durbin, P.A., Shabany, Y., Parneix, S. and Behnia, M. (1997), "Connections of Lagrangian dissipation theory to heat transfer", *2nd Int. Symposium on Turbulence, Heat and Mass Transfer*, Delft, The Netherlands, June, pp. 47-54.

Fusegi, T. (1996), "Numerical study of periodically-ribbed channel with oscillatory throughflow", *Proceedings of the 3rd International Symposium on Engineering Turbulence Modeling and Experiments*, Heraklion, Crete, Greece, 27-29 May, pp. 329-38.

Iacovides, H. and Raisee, M. (1997), "Computation of flow and heat transfer in 2-D rib roughened passages", *2nd International Symposium on Turbulence, Heat and Mass Transfer*, Delft, The Netherlands, 9-12 June, pp. 21-30.

Issa, R.I. (1985), "Solutions of implicitly discretized fluid flow equations by operator-splitting", *Journal of Computational Physics*, Vol. 62, pp. 40-65.

Kawamura, H. (1991), "A $k - \varepsilon - v^2$ model with special relevance to the near wall turbulence", *Proceedings of 8th Symposium on Turbulence Shear Flow*, Technical University of Munich, Munich, Germany, 9-11 September, pp. 26.4.1-26.4.6.

Lam, C.K.G. and Bremhorst, K. (1981), "A modified form of the $k - \varepsilon$-model for predicting wall turbulence", *Journal of Fluids Engineering, Transactions of the ASME*, Vol. 103, pp. 456-60.

Launder, B.E. and Sharma, B.I. (1974), "Application of the energy-dissipation model of turbulence to the calculation of flow near a spinning disc", *Letters in Heat and Mass Transfer*, Vol. 1, pp. 131-8.

Lin, C.A. and Hwang, C.B. (1998), "Improved low-Reynolds-number $k - \tilde{\varepsilon}$ model based on direct numerical simulation data", *AIAA Journal*, Vol. 36 No. 1, pp. 38-43.

Liou, T.M., Hwang, J.J. and Chen, S.H. (1993), "Simulation and measurement of enhanced turbulent heat transfer in a channel with periodic ribs on one principal wall", *Int. J. Heat Mass Transfer*, Vol. 36 No. 2, pp. 507-17.

Moin, P., Mansour, N.N. and Kim, J. (1988), "Reynolds stress and dissipation rate budget in turbulent channel flows", *Journal of Fluid Mechanics*, Vol. 194, pp. 15-44.

Patankar, S.V. (1980), *Numerical Heat Transfer and Fluid Flow*, Hemisphere Publishing Corporation, Washington, New York, London.

Patel, V.C., Rodi, W. and Scheuerer, G. (1985), "Turbulence models for near-wall and low-Reynolds number flow: a review", *AIAA Journal*, Vol. 23 No. 9, September, pp. 1308-19.

Taylor, C., Xia, J.Y., Medwell, J.O. and Morris, W.D. (1991), "Numerical simulation of three-dimensional turbulent flow and heat transfer within a multi-ribbed cylindrical duct", ASME Paper 91-GT-8, International Gas-Turbine and Aero Congress, Orlando, FL.

Tennekes, H. and Lumley, J.L. (1972), *A First Course in Turbulence*, The MIT Press, Cambridge, MA and London.

Tsai, W.B., Lin, W.W. and Chieng, C.C. (1997), "Effectiveness of preconditioning Bi-CGSTAB algorithm in solving turbulent flow", *Proceedings of the 10th International Conference*, Vol. 10, Swansea, 21-25 July, pp. 177-89.

van der Vost (1992), "Bi-CGSTAB: a fast and smoothly converging variant of Bi-CG for the solution of non-symmetric linear systems", *SIAM J. of Sci. Stat. Comp.*, Vol. 13 No. 2, pp. 631-44.

Wilcox, D.C. (1993a), "Turbulence modeling for CFD", DCW Industries, Inc., La Canada, CA.

Wilcox, D.C. (1993b), "A two-equation turbulence model for wall-bounded and free-shear flows", AIAA Paper 93-2905.

Wilcox, D.C. (1993c), "Comparison of two-equation turbulence model for bound layers with pressure gradient", *AIAA Journal*, Vol. 31 No. 8, pp. 1414-21.

Wilcox, D.C. (1994), "Simulation of transition with a two-equation turbulence model", *AIAA Journal*, Vol. 32 No. 2, pp. 247-55.

Wilcox, D.C. and Rubensin, W.M. (1980), "Progress in turbulence modeling for complex flow fields including effects of compressibility", NASA Tech. Paper 1517.

Yang, S.L., Chang, Y.L. and Arici, O. (1995), "Navier-Stokes computations of the NREL airfoil using a turbulent model at high angles of attack", *Journal of Solar Energy Engineering, Transactions of the ASME*, Vol. 117, pp. 304-10.

Yap, C.R. (1987), "Turbulence heat and momentum transfer in recirculating and impinging flows", PhD thesis, Department of Mechanical Engineering, UMIST, Manchester.